Quantitative measurement of the spectral function of aluminum and lithium by electron momentum spectroscopy

M. Vos, A.S. Kheifets, V.A. Sashin, and E. Weigold

Atomic and Molecular Physics Laboratories, Research School of Physical Sciences and Engineering, The Australian National University, Canberra ACT 0200, Australia

M. Usuda

Synchrotron Radiation Research Center, Japan Atomic Energy Research Institute, 1-1-1 Kouto Mikazuki-cho Sayo-gun Hyogo 679-5198, Japan

F. Aryasetiawan

National Institute of Advanced Industrial Science and Technology, Tsukuba, Ibaraki 305-8568, Japan

We present measurements of the spectral function of aluminum and lithium using high-energy electron momentum spectroscopy. For aluminum the quasiparticle peaks show clear asymmetries and significant satellite intensity that extends over a wide region to larger binding energies. The intensity distribution is not well described by band structure calculations. These data are described only by calculations based on the many-body cumulant expansion scheme. The measured momentum distribution at the Fermi level agrees with the theoretical one within 0.03 a.u. For lithium a bandwidth of 3.0 eV is obtained.

I. INTRODUCTION

The free-electron metals are considered to be among the simplest and best understood solids. Trivial models reproduce the main features of the band structure. This is surprising as the high density of electrons means that the interaction between them is significant, of the order of the band width. If one abandons the independent electron approximation, even these most simple of solids represent a huge theoretical challenge. In these theories the Coulomb electron-electron interaction is replaced by the screened electron-electron interaction.[1] The main differences between the independent electron theories and fully correlated theories that are, at least in principle, open to experimental verification are the following.

First, satellites appear at higher binding energy, both for valence band spectra and core level spectra.[2] These are interpreted in terms of plasmons, density fluctuations of the electron gas whose other effect is to screen the Coulomb potential of each electron. Most studies of these plasmon satellites are done by photoemission at high photon energies. A direct confrontation with theory is complicated by the presence of extrinsic plasmon effects, as well as questions related to the validity of the sudden approximation and the three-step model.[3]

Secondly, these correlations affect the momentum density. For a uncorrelated free-electron gas the momentum density jumps from a constant value to 0 at the Fermi momentum k_F. For a correlated electron gas this discontinuity is reduced, as for the intensity associated with the satellites there is no discontinuity at k_F. Momentum densities can be reconstructed from Compton profiles, obtained from x-ray scattering. For aluminum the Compton profiles show small deviations from the free-electron Fermi sphere and a discontinuity at k_F in agreement with theory.[4] However, in the case of lithium the asphericity is significant (k_F varying from 0.577 a.u. in the $\langle 100 \rangle$ direction to 0.604 a.u. in the $\langle 110 \rangle$ direction)[5] and the observed discontinuity at k_F is much smaller than current theories predict,[6] a problem that has attracted numerous different interpretations in recent years, see, e.g., the paper by Sternemann *et al.*, and references therein.[7]

In the third place electron-electron correlation changes the measured dispersion, and broadens the observed spectral lines.[8] Usually, the calculated band width decreases when electron-electron correlation is taken into account, in general agreement with the experiment,[9] however, the exact magnitude of this so called self-energy correction is difficult to extract from the experimental data due to the problems associated with the interpretation of low-energy photoemission data.[10,11] The real part of the calculated self-energy gives the self-energy correction to the band dispersion whereas the imaginary part describes the lifetime broadening. This can again be obtained by analyzing the line width in photoemission.[12] For photoemission the experimental resolution does not contribute significantly to the measured line width (except right at the Fermi level). In the case of free-electron metals the experimentally obtained line widths seem to exceed the theoretical estimates by about a factor of 2.[13]

If the electron-electron correlation is taken into account beyond a mean field level Bloch functions cease to be the eigenfunctions of the Hamiltonian. Removing an electron with momentum **q** creates an excited state with a broad distribution of energies. This distribution, which we call the spectral electron momentum density (SEMD), is given by the spectral function $A(\mathbf{q}, \omega)$.

Ideally one would like to measure the complete spectral function directly. Such a measurement would contain all the aforementioned phenomena plus much more as the intensity at each binding energy-momentum combination can be di-
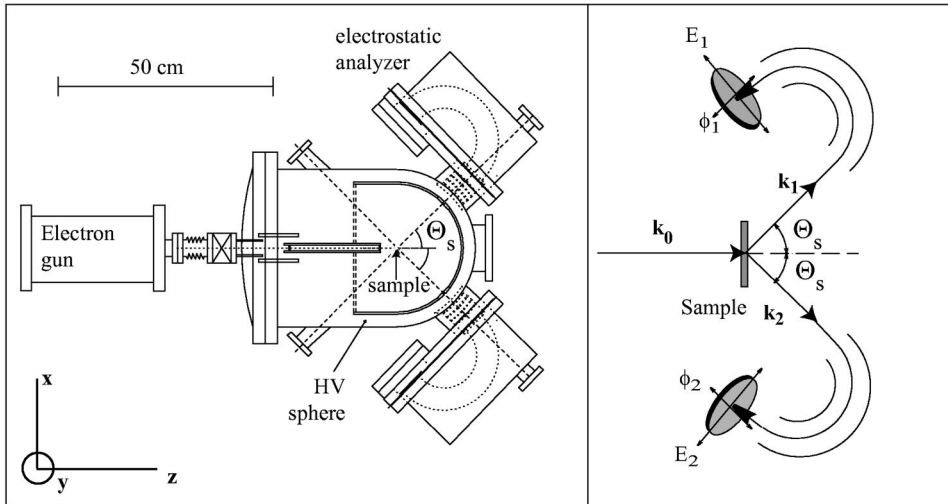
FIG. 1. An outline of the experimental setup (left) and scattering geometry (right).

rectly compared with the magnitude of the spectral function at these values. For example, the lifetime broadening of the spectra at a certain momentum value should be evident from a broadening of the feature as well as a reduction in the peak intensity. Satellite contributions will cause an additional reduction in the peak intensity of the quasiparticle peak.

In this paper we want to show that electron momentum spectroscopy (EMS) [an $(e,2e)$ measurement done under conditions where the plane-wave impulse approximation is valid] is a technique that is capable of doing such measurements of the spectral function for solids. In this respect EMS has great advantages over photoemission, where the experiment is tailored to a specific property of the spectral function one wants to measure. For example, photoemission intensities (corrected by matrix elements if required) are measured at high energies (XPS regime) whereas the dispersion of the valence band is measured at low energies (UPS regime) where the cross section can be very energy dependent.

II. EXPERIMENTAL DETAILS

The outline of the experimental apparatus is shown in Fig. 1. An electron gun with a barium oxide dispenser cathode emits a well collimated 25 keV electron beam. The sample is in a semisphere held at $+$ 25 kV. Thus 50 keV electrons impinge on the target. Symmetric $(e,2e)$ events are measured. The emerging pair of electrons with energies near 25 keV are decelerated and focussed at the entrance of hemispherical analyzers. These analyzers detect electrons emerging along part of a cone and over a range of energies using a two-dimensional channel plate–resistive anode based detection scheme. The scattering geometry is chosen such that, if all three electrons (incoming, labeled 0 and two outgoing, labeled 1 and 2) are in the same plane ($\phi_1 - \phi_2 = \pi$), then there is no momentum transfer from the target (or, in the single particle picture, one scattered from a stationary electron). In that case $\mathbf{k}_0 = \mathbf{k}_1 + \mathbf{k}_2$. If all three electrons are not in the same plane ($\phi_1 - \phi_2 \neq \pi$) there is an approximate vertical momentum component (out of the plane of Fig. 1) that corresponds to the recoil momentum of the system (which, in the single particle picture, corresponds to minus the momen-

tum of the struck electron.) The experimental apparatus and technique are described extensively elsewhere.[14,15]

A thin ($\simeq 30$ Å) free-standing carbon substrate covering a number of 0.3 mm diameter holes in the target mount was sputtered by argon ion etching until some of the films broke. Polycrystalline metal specimens were prepared by evaporating aluminum and lithium onto these foils. Aluminum was evaporated from a coil, whereas the lithium was deposited from a dispenser (supplied by SAES Getters). The thickness of the films were monitored by a crystal thickness monitor. This was done in a UHV preparation chamber, separate from the main spectrometer. After preparation the target specimens were transferred under UHV conditions to the spectrometer and measured. The pressure in the evaporation and sputtering chamber was of the order of 10^{-9} Torr and in the spectrometer itself the operating pressure was about 3×10^{-10} Torr.

As we want to compare quantitatively the EMS experiment with the theoretical description of the electronic structure we want to discuss here at some length the effect of finite energy and momentum resolution on these measurements. We will do this by simulating the experimental data for a fictitious free-electron solid (without electron correlation). Within this model we know the energy of the electron ε if we know the momentum $\mathbf{p}$ of the electron. Hence we do not have four independent variables ($p_x, p_y, p_z, \varepsilon$) but only three. As we will see this means that the position of the peaks in the energy spectra can be affected by the momentum resolution, and vice versa that the value of the momentum with maximum intensity at a certain binding energy is affected by the energy resolution.

In practice we know the incoming energy accurately (0.3 eV thermal spread, plus possible space charge broadening), hence the magnitude of the incoming momentum vector $\mathbf{k}_0$ is fixed with extremely high precision, and we have uncertainties only in the direction of propagation. Thus the error vector $\Delta\mathbf{k}_0$ is directed perpendicular to $\mathbf{k}_0$. In our experiment the collimation is achieved by two circular apertures, 0.4 and 0.1 mm in diameter, 215 mm apart. We can calculate the transverse momentum distribution of the beam if we assume that the position at which the electron passes through the first aperture is uncorrelated with the position at which it passes

through the second. For a 50 keV electron (momentum 62.07 a.u.) the root-mean square (σ) of the error in each of the two perpendicular directions (x and y, see Fig. 1) is 0.030 a.u. (1 a.u. of momentum corresponds to 1.89 Å^{-1}.) Note that the error distribution deviates from Gaussian, it has a relatively flat top followed by a sharp drop.

By the same token we know with high precision the magnitude of the momentum of the scattered and ejected electron, but there is a small uncertainty in the direction of propagation. These measurements were done with 0.5 mm slits 150 mm away from the target. This corresponds to a root-mean square of error in the direction perpendicular to the slits of 0.043 a.u.

In the direction perpendicular to the plane (y direction), the momentum resolution is determined by the accuracy of the angular detection. To determine this accuracy we place a set of narrow circular apertures (0.1 mm diameter) in front of the 0.5 mm slits. The width of the angular distribution measured in this way is 0.03°, corresponding to a momentum resolution of 0.024 a.u.

For convenience we will approximate the momentum error distribution to be Gaussian. Adding the error of the incoming and outgoing electrons in quadrature we get $\sigma(p_x)$ $=0.052$ a.u., $\sigma(p_y)=0.045$ a.u., and $\sigma(p_z)=0.043$ a.u.

We now calculate the spectra for a free electron model using these momentum resolution values and an energy resolution of 1 eV, derived from our core level measurements, as described in Sec. IV A. We consider a set of grid points p_x, p_y, p_z inside the Fermi sphere with a separation smaller than the momentum resolution (and the maximum energy separation of adjacent points smaller than the energy resolution). The binding energy at each point is $\varepsilon(p_x, p_y, p_z)$. The measured intensity I at binding energy E and momentum p_x, p_y, p_z is then given by

$$I(E, q_x, q_y, q_z)$$

$$= \sum_{p_x, p_y, p_z} C e^{-(p_x - q_x)^2/2\sigma_{p_x}^2} \; e^{-(p_y - q_y)^2/2\sigma_{p_y}^2}$$

$$\times e^{-(p_z - q_z)^2/2\sigma_{p_z}^2} \; e^{-[\varepsilon(p_x, p_y, p_z) - E]^2/2\sigma_E^2}. \tag{1}$$

Resolutions quoted in the remainder of the paper refer to the full width at half maximum (FWHM), rather than the standard deviation σ. Thus our experimental momentum resolution is thus (0.12, 0.10, 0.10 a.u.) for the x, y, z direction. In Fig. 2 we show a set of simulated spectra as a function of q_y, ($q_x, q_z = 0$) summed over intervals in q_y of 0.1 a.u. for a noninteracting free electron gas with k_F $=0.93$ a.u. as appropriate for aluminum. Near $q_y = 0$, where the band energy changes little with q, the width of the spectra is determined solely by the energy resolution. At larger momentum values, where the binding energy starts decreasing more and more rapidly with increasing momentum, the spectra broaden, due to finite momentum resolution. Note that even near k_F the spectra peak significantly above zero binding energy. The peak position in the spectra corresponds to the average binding energy of all states that contribute to the
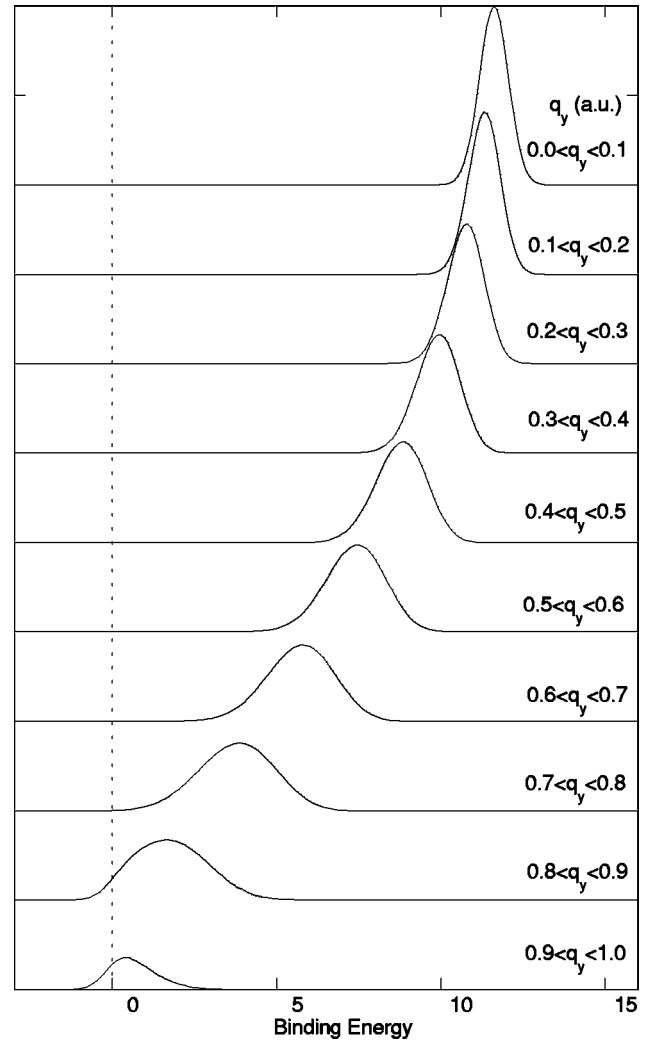

FIG. 2. Spectra at different momentum intervals as simulated with experimental momentum and energy resolution. A free electron model with $k_F = 0.93$ a.u. was assumed $q_x, q_z = 0$, q_y as indicated.

intensity, and states with negative binding energies do not contribute to the intensity, as they are unoccupied.

In Fig. 3 (top panel) we explore further the effects of varying the energy and momentum resolution on the simulated data. If we have no momentum resolution the curve corresponds to the familiar inverted parabola of the density of states of a free-electron gas as measured by XPS.[16] At zero binding energy the intensity is 0.5 times the maximum intensity. If we have a modest momentum resolution of 0.2 a.u. along each p_x, p_y, and p_z direction, then we get a spectrum at $|q| = k_F$ that peaks near 0.7 eV binding energy. The peak is at an energy value close to the average of all the states that contribute. Only if the momentum resolution is very good (0.05 a.u.) do we get a spectrum at $|q| = k_F$ that peaks very close to 0 eV.

Similar effects apply to the momentum profiles which are illustrated in Fig. 3 (bottom panel). With no energy resolution and momentum resolution in only one direction, the data are the familiar semicircle results, as obtained for Compton scattering from a noninteracting free-electron gas.[17] With momentum resolved in all three directions, but without en-

Spectra at k_F=0.93 a.u.
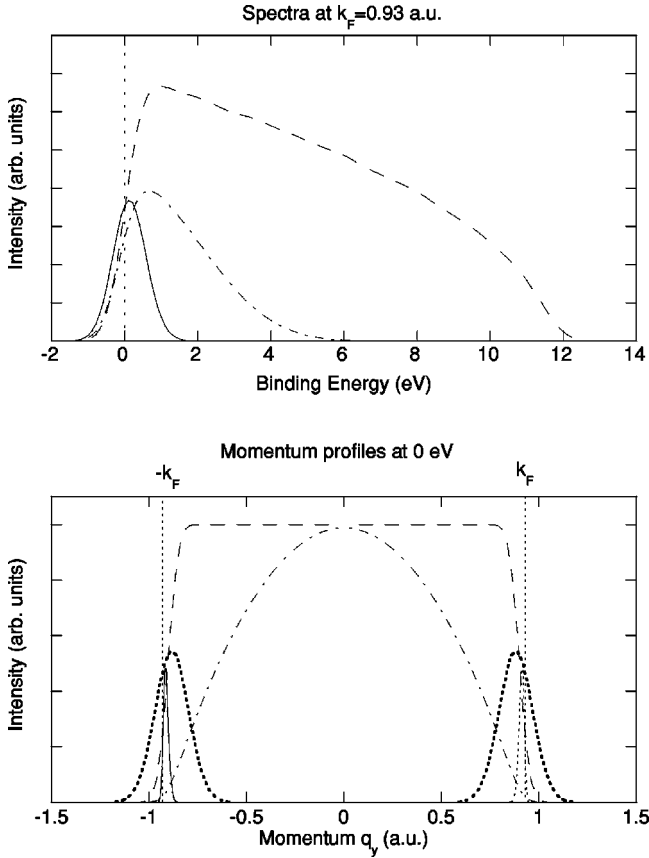

Momentum profiles at 0 eV

FIG. 3. The effect of different values of momentum and energy resolution on the simulated spectra and momentum densities for a free electron gas with the same electron density as aluminum (k_F =0.93 a.u.). In the top panel we show the spectra as obtained at $\mathbf{q}=(k_F,0,0)$ without momentum resolution (dashed line), poor momentum resolution (isotropic, 0.2 a.u.) (dash-dotted line) and good momentum resolution (isotropic, 0.05 a.u.) (solid line). In all three cases the energy resolution was 1 eV. In the bottom panel we show momentum profiles for (a) no energy resolution and no resolution in q_x,q_z but a resolution in $q_y=0.1$ a.u. (dash-dotted line), (b) no energy resolution, momentum resolution isotropic, 0.1 a.u. (long dashed line), (c) energy resolution 1 eV, momentum resolution 0.2 a.u. isotropic (short dashed line), and (d) energy resolution 1 eV, momentum resolution isotropic, 0.05 a.u. (full line).

ergy resolution, the data resemble momentum densities as obtained by $(\gamma,e\gamma)$ experiments.[18] With an energy resolution of 1 eV and modest momentum resolution the peaks in the distribution at the Fermi level are found at momentum values significantly smaller than k_F. Only if the momentum resolution is improved from 0.2 to 0.05 a.u. does the peak position coincide with k_F.

In summary, there is an interplay between the energy resolution and the momentum resolution vector. For accurate extraction of parameters from these measurements it is crucial that these effects are taken into account.

III. THEORY

In an $(e,2e)$ collision process the energies and momenta of the incident and two outgoing electrons, detected in coin-

cidence, are fully determined. Thus from energy and momentum conservation one can determine the separation or binding energy of the ejected electron

$$\omega=E_0-E_1-E_2 \qquad (2)$$

and the recoil momentum of the ionized specimen

$$-\mathbf{q}=\mathbf{k}_1+\mathbf{k}_2-\mathbf{k}_0. \qquad (3)$$

At high energies the incident and outgoing electrons can be treated as free electrons, i.e., plane waves for a homogeneous free-electron-like system (or as Bloch waves for a single crystal lattice). [At high energies inside the solid the interaction between the plane wave and the surroundings is significant, and its energy level is broadened significantly (several eV's). This causes additional broadening in Compton spectroscopy.[6] In EMS, the electrons are detected outside the material where their energies are well defined, and no complications arise.] Also at high energies the momentum transfer $\boldsymbol{\kappa}=\mathbf{k}_0-\mathbf{k}_1$ can be made large. Thus the size of the area from which the electron is scattered $\sim\kappa^{-1}$ can be made very small, ensuring that the collision is with a single electron. The maximum possible value of κ is $k_0/\sqrt{2}$ since the electrons are indistinguishable. Thus for 50 keV incident electrons $\kappa^{-1}\sim0.02a_0$, ensuring a clean electron-electron or binary collision. Under these conditions the recoil momentum is equal and opposite to the momentum the final state consisting of a single hole in the interacting (N) electron system. Since $|\mathbf{q}+\boldsymbol{\kappa}|\gg k_F$ we can neglect exchange between the bound and free electrons because the overlap between the high momentum free electrons with the low momentum ($q \lesssim k_F$) bound electrons is vanishingly small.

The differential cross section is then given by[19,20]

$$\sigma(\mathbf{k}_0,\mathbf{k}_1,\mathbf{k}_2,\omega)=(2\pi)^4\,\frac{k_1k_2}{k_0}f_{ee}A(\mathbf{q},\omega), \qquad (4)$$

where the full spectral electron momentum density is given by

$$A(\mathbf{q},\omega)=\pi^{-1}G^-(\mathbf{q},\omega). \qquad (5)$$

Here $G^-(\mathbf{q},\omega)$ is the single-hole (retarded) Green's function of the many electron target. f_{ee} is the electron-electron scattering cross section, which is proportional to κ^{-4} (in the Born and plane wave impulse approximations) and thus constant in the noncoplanar geometry where $\theta_{1,2}$ and $k_{1,2}$ are kept fixed and the azimuthal angle $\phi_{1,2}$ are varied to vary $\mathbf{q}$. The optimal arrangement for maximizing κ is to have $\theta_1 =\theta_2\approx45°$ and $k_1=k_2$ and varying ϕ_1 and ϕ_2 where the angles θ and ϕ are defined relative to $\mathbf{k}_0$.[20]

Presuming that the Green's function can be diagonalized on an appropriate basis of momentum space quasiparticle states ϕ_i (electron shells in atoms, Bloch waves in crystals, etc.) one can write Eq. (5) as

$$A(\mathbf{q},\omega)=\sum_i\,|\langle\mathbf{q}|\phi_i\rangle|^2\pi^{-1}G_i^-(\omega). \qquad (6)$$

The imaginary part of the single-hole Green's function is calculated as

$$\text{Im}\,G_i^-(\omega)=\sum_\alpha\,|\langle N-1,\alpha|\hat{a}_i|N,0\rangle|^2\delta(\omega-E_{N-1,\alpha}+E_{N,0}),$$
(7)

where $\hat{a}_i$ is the annihilation operator which removes an electron defined by the quantum label i from the ground state of the system of N interacting electrons $|N,0\rangle$, leaving a state which is a superposition of the eigenstates of the ionized system $|N-1,\alpha\rangle$. Only those states contribute which are compatible with energy conservation and which overlap with the one-hole state. For an extended system (crystal) momentum conservation requires Eq. (5) to take the form

$$A(\mathbf{q},\omega)=\sum_{i,\mathbf{k},\mathbf{G}}\,|\langle\mathbf{q}|\phi_{i\mathbf{k}}\rangle|^2\delta_{\mathbf{q},\mathbf{k}+\mathbf{G}}\,\pi^{-1}\text{Im}\,G_i^-(\mathbf{k},\omega).$$ (8)

Here i is the band index, $\mathbf{k}$ the crystalline momentum, and $\mathbf{G}$ the reciprocal lattice vector.

In the absence of electron-electron interactions the noninteracting Green's function is just a delta function $\pi^{-1}\text{Im}\,G_i^{-(0)}(\mathbf{k},\omega)=\delta(\omega-\omega_{i\mathbf{k}})$, and the SEMD contains only one delta-function line following the band dispersion. The interacting SEMD Eqs. (5)–(7) contain much more information than the simple band dispersion. The main feature in $\text{Im}\,G_i^-(\mathbf{k},\omega)$ describes the quasiparticle in band i having momentum $\mathbf{k}$ and energy ω. The center of the quasiparticle peak is shifted with respect to the one-electron energy $\epsilon_{i\mathbf{k}}$ and the peak acquires a width due to the finite quasiparticle lifetime. Additional satellite structures arise in the SEMD due to the electron-electron correlations. All this can be directly measured in EMS through the cross section given in Eq. (4).

It is important to note that the momenta $\mathbf{q}$ measured in EMS are real momenta [Eq. (3)] and not crystal momenta. The crystal momentum does not appear in the expression for the cross section. Thus EMS works equally well for polycrystalline and amorphous materials, as well as for single crystals. This makes EMS a probe that can test jellium-type calculations of free-electron materials such as aluminum, since the crystal lattice potential is not an essential part of the excitation process. However, except for the case of single crystal specimens, there is in general no preferred direction in space, and the cross section measures a spherically averaged $A(q,\omega)$. Also, in contrast to photoemission experiments the EMS cross section is simple to interpret since there are no different matrix elements for different electrons (s,p, etc.) and the emitted electrons are of high enough energies ($E_i\gg 1$ keV) that they can be treated accurately (e.g., as plane waves or Bloch waves).

Electron correlations models. The one-hole Green's function entering Eq. (8) can be calculated by the many-body perturbation theory (MBPT) expansion on the Bloch wave basis as obtained from an LMTO (linear muffin tin orbital) calculation. Taking the first nonvanishing term in the MBPT leads to the so-called *GW* approximation.[1,21] G is the Green's function and W denotes the screened Coulomb interaction.

The *GW* approximation is known to give accurate quasiparticle energies.[22] However, its description of satellite structures is not satisfactory. In alkali metals, for example, photoemission spectra show the presence of multiple plasmon satellites whereas the *GW* approximation yields only one at too large an energy. This shortcoming of the *GW* approximation has been resolved by introducing vertex corrections in the form of the cumulant expansion to the Green's function.[23–25] This allowed the inclusion of multiple plasmon creation. As a result the calculated peak positions of the plasmon satellites were found to be in much better agreement with the experiment than those predicted by the *GW* scheme itself.[26–28]

Formally, the cumulant expansion for the one-hole Green's function can be derived as follows. We choose the time representation for the Green's function, drop the band index i for brevity, and write it as

$$G(\mathbf{k},t<0)=i\,\theta(-t)e^{-i\omega_k t+C^h(\mathbf{k},t)},$$ (9)

where ω_k is the one-electron energy and $C^h(\mathbf{k},t)$ is defined to be the cumulant. Expanding the exponential in powers of the cumulant we get

$$G(\mathbf{k},t)=G_0(\mathbf{k},t)\left[1+C^h(\mathbf{k},t)+\frac{1}{2}[C^h(\mathbf{k},t)]^2+\cdots\right],$$
(10)

where $G_0(\mathbf{k},t)=i\,\theta(-t)\exp(-i\omega_k t)$. In terms of the self-energy Σ, the Green's function for the hole can be expanded as

$$G=G_0+G_0\Sigma\,G_0+G_0\Sigma\,G_0\Sigma\,G_0+\cdots.$$ (11)

To lowest order in screened interaction W, the cumulant is obtained by equating

$$G_0 C^h=G_0\Sigma\,G_0,$$ (12)

where $\Sigma=\Sigma_{GW}=iG_0 W$. The first-order cumulant is therefore

$$C^h(\mathbf{k},t)=i\int_t^\infty dt'\int_{t'}^\infty d\tau e^{i\omega_k\tau}\Sigma\,(\mathbf{k},t).$$ (13)

This is then put back into Eq. (9) yielding multiple plasmon satellites. The energy-momentum representation of the Green's function can be restored by the time Fourier transform.

For comparison with the EMS measurements, which were taken on polycrystalline samples as discussed in Sec. IV, the calculated SEMD's were spherically averaged and the known energy and momentum resolutions were convoluted onto the theoretical SEMD's. For these free-electron-like materials the effects of spherically averaging is small. For more covalent materials the spherical averaging will result in broadening of the features, and loss of direct information of the anisotropy of the spectral function.
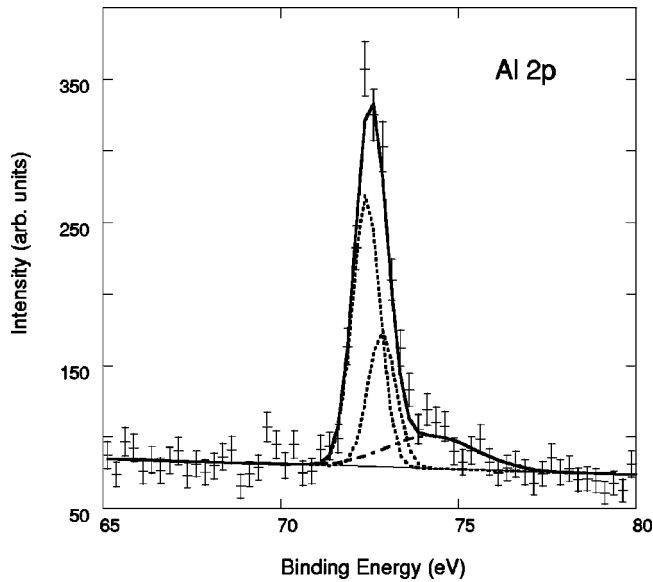
FIG. 4. The Al $2p_{3/2,1/2}$ binding energy spectrum (relative to the Fermi level) integrated over the momentum range 0–3 a.u. The two short-dashed peaks show the $2p_{3/2}$ and $2p_{1/2}$ contributions of width 0.9 eV, separation of 0.4 eV, and statistical weight of 2:1. The long dashed peak is due to oxide formation and the thin line is a fit to the background produced by inelastic scattering of the electrons.

IV. RESULTS

A. Aluminum

To illustrate the energy resolution of the spectrometer we show in Fig. 4 the $2p$ core level of aluminum. The spectrum was obtained by integrating the experimental data over a wide momentum range. This level has a spin-orbit splitting of $\simeq 0.4$ eV as known from photoemission.[29] The EMS data were fitted using this value of the spin-orbit splitting and a second, broader component due to aluminum oxide, as some oxidation of the sample cannot be avoided during the 24 h of the measurement.[29,30] In this way we obtain experimentally

an energy resolution of 0.9 eV. The dependence of the cross section on the momentum is proportional to the modulus square of the $2p$ momentum space wave function. A comparison of the $2p$ and $2s$ intensity distribution with the atomic Al $2p$ and $2s$ wave function was given elsewhere.[31]

In Fig. 5 we show the measured intensity as a function of energy and q_y component of the momentum ($q_x = q_z = 0$). In the left panel we show the raw data. A parabolic feature (the quasiparticle band) stands out clearly. At the high binding energy side of this band the intensity drops off only slowly. This is to a large extent due to inelastic multiple scattering. In these multiple scattering cases the incoming and/or one of the outgoing electrons experience some energy loss, e.g., by plasmon excitation, and the binding energy as inferred from Eq. (2) is too high. The level of multiple scattering in the sample was measured in a separate experiment by tuning the energy of the incoming beam to the detection energy of the analyzer. All electrons detected under these conditions have been scattered over an angle near $44.3°$. Some of them lost energy due to excitation of a plasmon. The likelihood of plasmon excitation increases with sample thickness. These energy loss spectra are shown in Fig. 6.

The shape of the energy loss spectrum (loss function) can be fitted empirically. Now we assume that the inelastic energy loss distribution of the EMS measurement is described by the same loss function. The probability of inelastic multiple scattering in the EMS experiment and the energy loss experiment are directly related, as described in detail by Vos *et al.*[32] Hence after measuring the loss function, we can, using the empirical fit of the loss spectrum, and the intensity ratio of the "zero-loss elastic scattering contribution" and the "elastic scattering plus energy loss contribution" deconvolute the measured EMS spectrum without any free parameters. The result is shown in the right panel of Fig. 5.

After deconvolution the intensity approaches zero more quickly below the quasiparticle band. However significant intensity extends way beyond the quasiparticle peak. This is sometimes referred to as the so-called plasmaron[33] (or intrin-
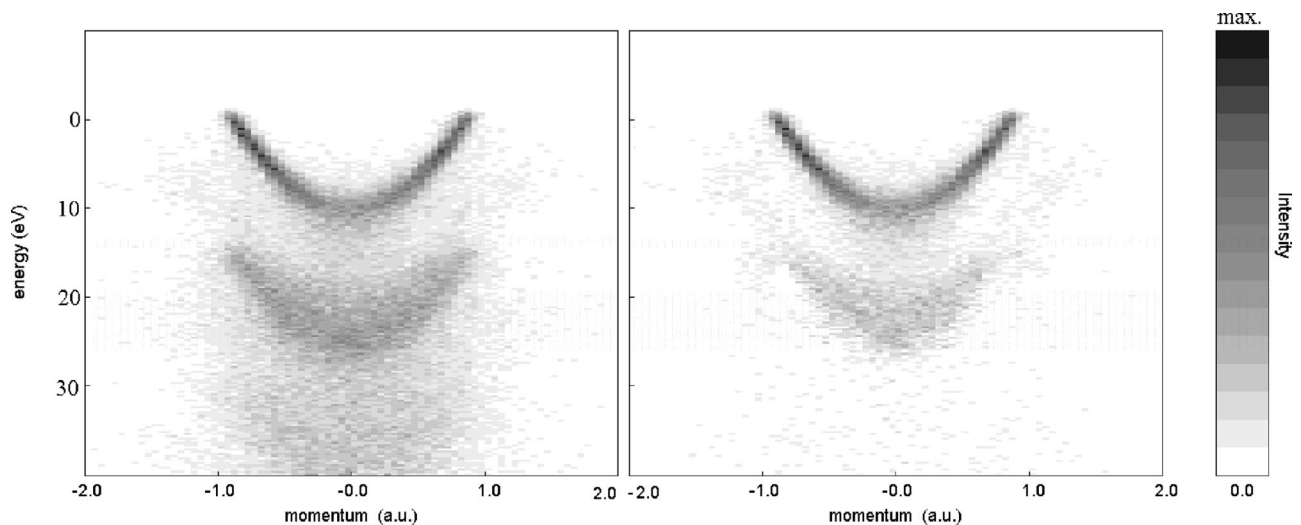
FIG. 5. The measured spectral momentum density (SEMD) in the region of the conduction band of aluminum before (left) and after (right) deconvolution for inelastic multiple scattering. The density is shown as a linear gray scale.
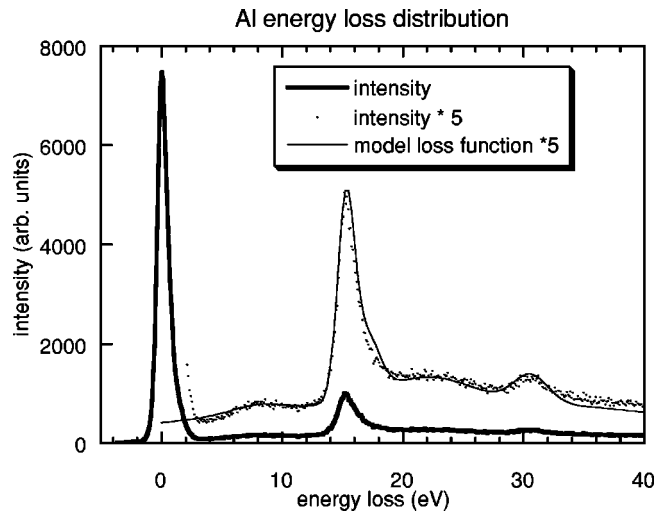
FIG. 6. The measured energy loss spectrum of 25 keV electrons scattered elastically from an Al foil over 44.3°. The intensity at 15.2 and 30.5 eV energy loss are due to single and double plasmon creation, respectively. The fitted "loss function" is used to correct the EMS data for inelastic multiple scattering as described in the text.

sic plasmon) part of the spectrum. It comprises a significant part of the total intensity. A requirement for a valid deconvolution procedure is that no significant negative intensities appear anywhere in the deconvoluted spectra. Our procedure meets this requirement as illustrated in Fig. 7, for valence band spectra at different momentum values.

In the top panel of Fig. 7 we extend this analysis to the $2s$ and $2p$ core level region. The $2p_{3/2,1/2}$ and $2s$ core levels are clearly visible at $\omega = 72.5$ and 117.5 eV, respectively, above an essentially smooth background tail due to multiple inelastic scattering from the conduction band. Also visible are peaks due to energy loss by excitation of one or two plasmons. These plasmons can be created as part of the core hole creation event (intrinsic excitation) or by the passage of the high-energy electrons through the foil (extrinsic plasmon). The latter contribution is removed by the deconvolution process. In the discussions of plasmon intensities of core levels in photoemission experiments, one also assumes a multistep model, i.e., one assumes that the creation of the hole (which includes the creation of intrinsic plasmon satellites) can be separated from the propagation of the photoelectron to the surface (which may involve the creation of extrinsic plasmons) and its subsequent escape from the surface. Based on this model Hüfner[16] compiled creation rates of intrinsic plasmons (satellite intensities) for the Al $2p$ core state which ranged from 11 to 34 % of the main line. Subtracting the extrinsic plasmon contribution, by deconvolution for inelastic scattering as discussed above, we obtain the spectrum shown by the solid line in the top panel of Fig. 7. This gives intrinsic satellite intensities of 30 and 17 % of the main line for respectively the $2p$ and $2s$ states, values in the same range as the photoemission results.

The middle and bottom panels of Fig. 7 show the results of deconvolution for the conduction band near the Fermi edge ($q_y \sim 0.9$ a.u., quasiparticle peak near 0 eV binding en-
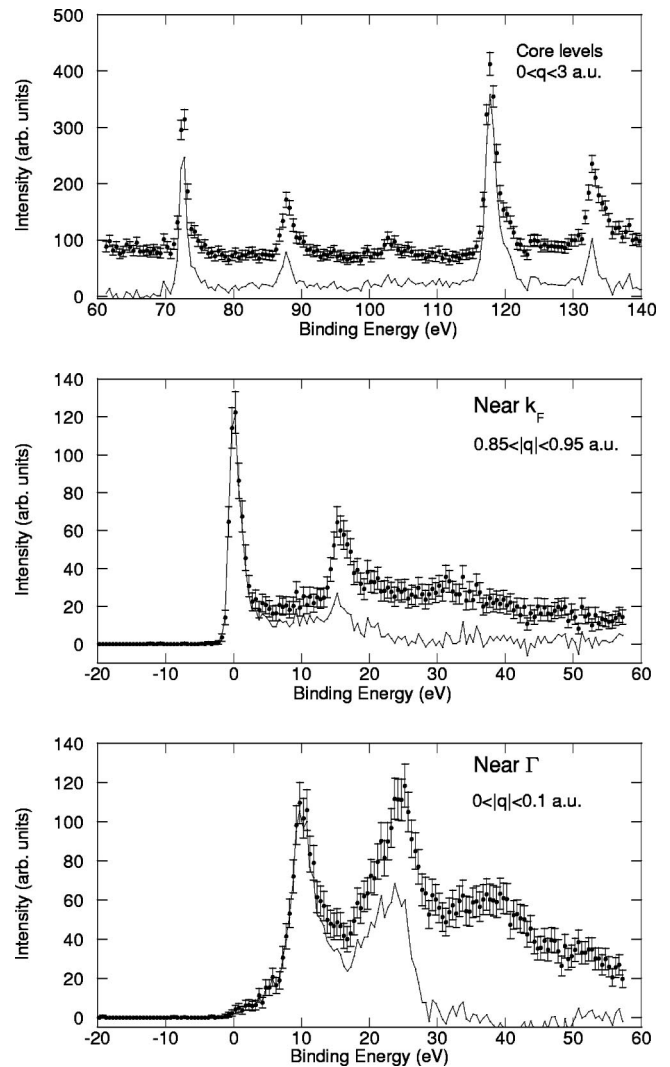

FIG. 7. Binding energy spectra for Al showing the raw data (error bars) and the data deconvoluted for inelastic scattering processes such as excitation of extrinsic plasmons (solid line). The top panel shows the spectra in the core region summed over all momenta from 0 to 3 a.u. The $2p_{3/2,1/2}$ peak at ~ 72.5 eV and $2s$ peak at ~ 117.5 eV. Each peak is followed by a plasmon satellite at 15 eV higher binding energy. The middle and bottom panels show the outer (conduction) band region at, respectively, the Fermi edge ($q_y \sim 0.9$ a.u., $q_x, q_z \simeq 0$ a.u.) and near the Γ point (**q** ~ 0) a.u.

ergy) and near the Γ point, respectively ($q_y \sim 0$ a.u., quasiparticle peak near 12 eV binding energy). Again the intensity extends well beyond the quasiparticle peak, approaching zero at binding energies exceeding 30 eV. There is a distinct difference in shape between the loss feature near k_F and near Γ. Deconvolution removes most of the sharp peak near k_F but much of the broad satellite at Γ remains. Thus there is clear experimental evidence, that for the valence band, the intrinsic satellite has a different shape near k_F than near Γ. Near Γ the screening related satellite is much stronger, reflecting the fact that electrons with $q=0$ are more effectively screened than electrons with large momenta.[34] Also the quasiparticle feature is much broader at Γ than at k_F.
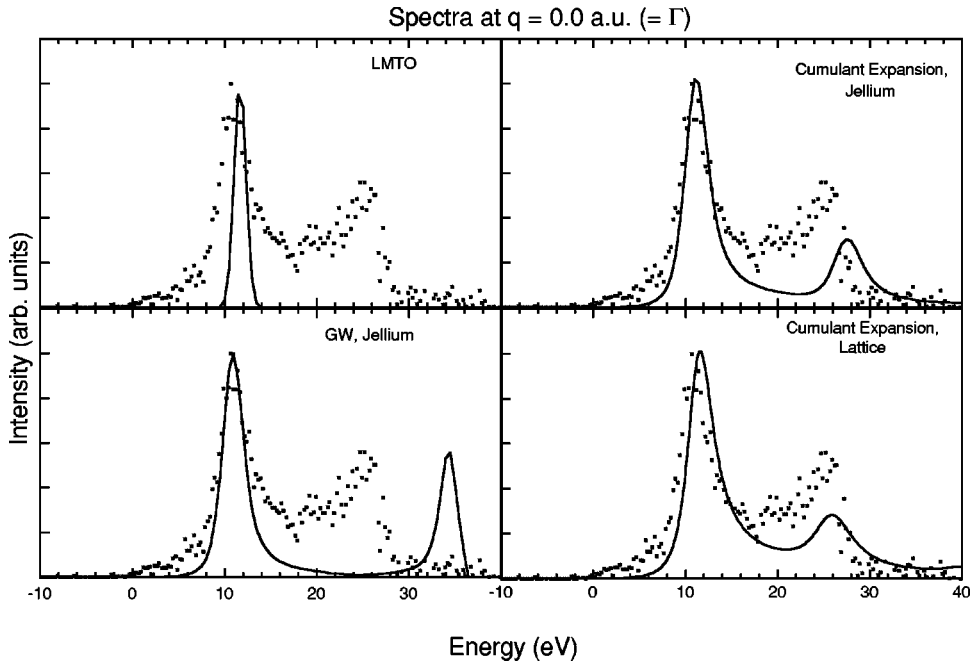
Spectra at q = 0.0 a.u. (= Γ)

FIG. 8. The deconvoluted measured SEMD for Al at zero momentum compared with four different theories. All theories are broadened with the energy resolution. The width of the LMTO theory is equal to the experimental resolution. Further details are described in the text.

In our simulations of the spectra for a noninteracting free electron gas (Fig. 2) the highest intensities and the sharpest peaks are near zero momentum. In contrast for the measurement the highest and sharpest peaks are found near the Fermi level. This is because lifetime broadening was not included in the model calculations.

The deconvolution has removed approximately the effects of inelastic scattering but the effects of elastic scattering (deflection of an incoming or either of the outgoing electrons by a target nucleus) are still present. For a noninteracting electron gas the momentum density decreases discontinuously from a constant value to zero at k_F. For an interacting electron gas this discontinuity at k_F is reduced. In principle this could be studied by EMS by plotting the momentum density integrated over all binding energies. However elastic scattering causes a decrease of the measured step at k_F as well. Therefore it is currently not possible to use these EMS data to study the discontinuity of (the energy-integrated) momentum density at the Fermi momentum k_F.[28]

After deconvolution for inelastic scattering it became clear that a small part of the spectrum was due to the supporting carbon film. The SEMD of carbon is well known[35] and it extends to higher momentum values ($\simeq 1.5$ a.u. compared to $\simeq 1.0$ a.u. for aluminum). Therefore by examining the intensity of the characteristic carbon features at higher momenta, we can decide on the magnitude of carbon signal to subtract. This is a relatively minor correction.

We now compare the deconvoluted spectra with four different calculations. This is done in Fig. 8 for the spectra near zero momentum. The LMTO calculation is a band structure type calculation, and hence electron-electron interaction is taken into account only at a mean-field level. No life time broadening is predicted by this theory, but the peak position (12 eV binding energy) is close to the peak position of the experiment. The peak width has been artificially broadened to match the experimental energy resolution.

A *GW* calculation based on a jellium model with the same electron density as aluminum predicts again a peak at the right position. In the jellium model the lattice is replaced by a homogeneous positive charge density, i.e., there is no periodic potential. Now the calculation predicts lifetime broadening and satellite intensity at higher binding energies. However, the satellite position is as much as 10 eV higher in binding energy than the experiment, and in between the satellite and the quasiparticle peak the calculated intensity is close to zero in the theory, whereas the experiment has significant intensity in this energy range.

Significant improvement is obtained if the *GW* scheme is replaced by the cumulant expansion scheme. First we consider the cumulant expansion scheme for a jellium with the same electron density as Al. Now the quasiparticle peak becomes more asymmetric, with a significant tail at the high-binding energy side. Most importantly the position of the satellite is now much closer to the experimentally observed position. In this calculation the changes to the quasiparticle band width due to self-energy effects were small (<0.2 eV).

Finally we can do the cumulant expansion calculation based on a crystal lattice. For the uncorrelated electron gas of a jellium the eigenfunctions are plane waves. Electron-electron correlations are then introduced as a kind of perturbation, using the plane waves as a basis. Similarly one can use the Bloch functions, as obtained from the full-potential LMTO code as a starting point. This approach results in an even more asymmetric and broader quasiparticle peak with significant intensity all the way up to the satellite. Indeed it gives much better agreement with the experiment. The experiment has some intensity at lower binding energy than the quasiparticle peak, all the way up to 0 eV. This intensity is a known artifact due to elastic multiple scattering as explained by Vos and Bottema.[36] The observed discrepancy at the higher binding energy side has no known cause. It may either
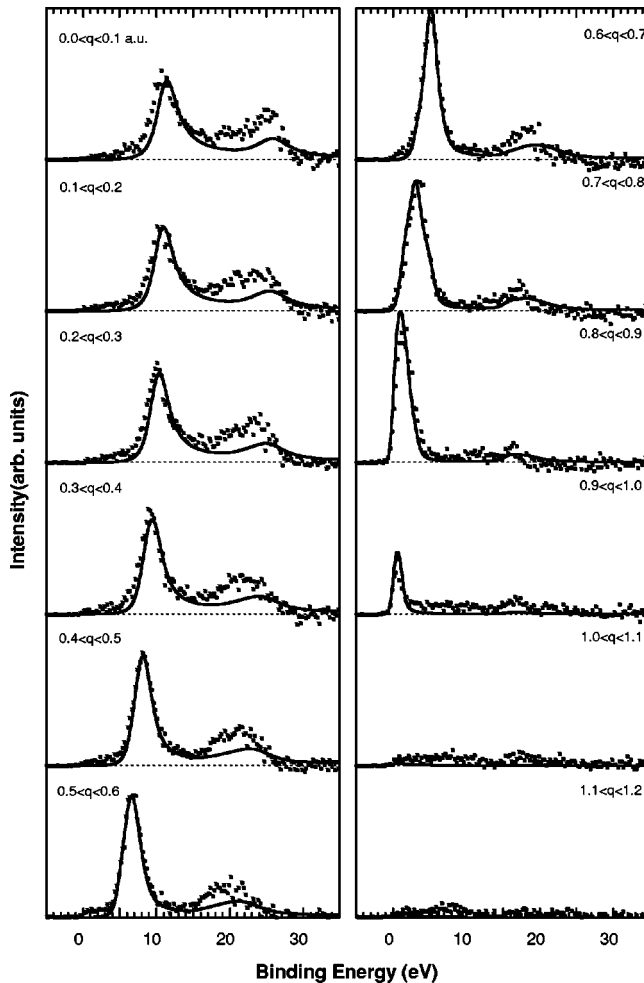
FIG. 9. The deconvoluted measured SEMD for Al at different momenta compared with the many-body cumulant expansion theory (smooth solid line). The theory was broadened with the experimental energy resolution (1.0 eV) and the momentum resolution vector (0.12, 0.1, 0.1 a.u.). A single scaling factor is used for comparison of experiment and theory.

be a shortcoming of the calculation, requiring the inclusion of more diagrams, or due to shortcomings in the deconvolution procedure.

It could be argued that the agreement between the last theory and experiment in the spectra taken at zero momentum is somewhat accidental. It is therefore essential to compare the measured and calculated spectra over the whole range of momenta. This is done in Fig. 9 for the deconvoluted experiment and the cumulant expansion theory, based on Bloch functions. The calculation was convoluted with the experimental energy and momentum resolution as described by Eq. (1). The agreement over the whole range of momenta is striking.

Note that for low momentum values ($q_y < 0.3$ a.u.) the quasiparticle line shape is clearly asymmetric, both in theory and experiment, i.e., the low binding energy side is noticeably steeper than the high-binding energy side. This is at variance with the photoemission results[13] that claim a symmetric peak shape near Γ, possibly due to the larger degree in freedom in subtraction of the large background in the photoemission case.

B. Lithium

Compared to aluminum it is experimentally more difficult to keep the Li film clean during the EMS experiment. A clear signal related to lithium oxide develops quickly. The lithium quasiparticle intensity, however, is easily identified by its characteristic parabolic dispersion, and is at smaller binding energies than the lithium oxide related features. The momentum profiles of the Li metal are shown in Fig. 10. Unfortunately at larger binding energies, below the quasiparticle band, the contribution of the lithium oxide becomes significant and hence it is not possible to extract meaningful information about the presence of satellites from these data.

In the left panel the experimental data are compared with simulated densities for a free-electron metal with $k_F = 0.589$ a.u., the appropriate value for a free electron solid with the electron density of Li. However, the corresponding band width of 4.7 eV is clearly too large. Hence we used the effective electron mass m^*, as a fitting parameter. In the calculation plotted in the left panel we used $m^* = 1.6 m_e$ and the corresponding band width is 3.0 eV. This band width gives a good description of the peak positions in the measured momentum profiles. This value is also in good agreement with the x-ray absorption measurements [3.0 ± 0.1 eV (Ref. 37)] and the photoemission data (between 2.8 and 3.2 eV, depending on the method of analysis[11]). Agreement between the simulated spectra and the measured ones is quite good, and the main deviations can be understood in terms of a small, rather uniform background at higher binding energy due to the tail of the oxygen feature at slightly larger binding energy, and the effect of lifetime broadening on the experimental data near the bottom of the band. Broadening of the levels in energy leads to an apparent broadening of the momentum profiles and hence a reduction in maximum intensity.

In the central panel of Fig. 10 we compare the measurement with a cumulant expansion theory using the LMTO description of the lithium crystal as starting point. The result of the calculation was corrected for finite energy and momentum resolution of the spectrometer, as described before. It turned out that the real part of the self-energy correction was rather small ($\simeq 0.2$ eV) and was put to zero. However, due to the asymmetry of the line shape, the position of maximum intensity shifts from $\simeq 3.5$ to 3.8 eV. This approach clearly gives a band width that is too large (3.8 eV) and applying the calculated self-energy correction only improves the situation marginally.

In the right panel of Fig. 10 we plot the same theory, but now with an energy scale contracted by 20%. In this way the total band width is again near 3 eV. The peak positions are very similar to those obtained from the free electron model. However, due to the lifetime broadening the maximum intensity at higher binding energy is lower, the momentum profiles are broader at these energies as well. Indeed the calculated intensity is close to the measured one, at all binding energies, except for the background gradually increasing with binding energy, due to the tail of the oxygen contribution centered at slightly higher binding energies.
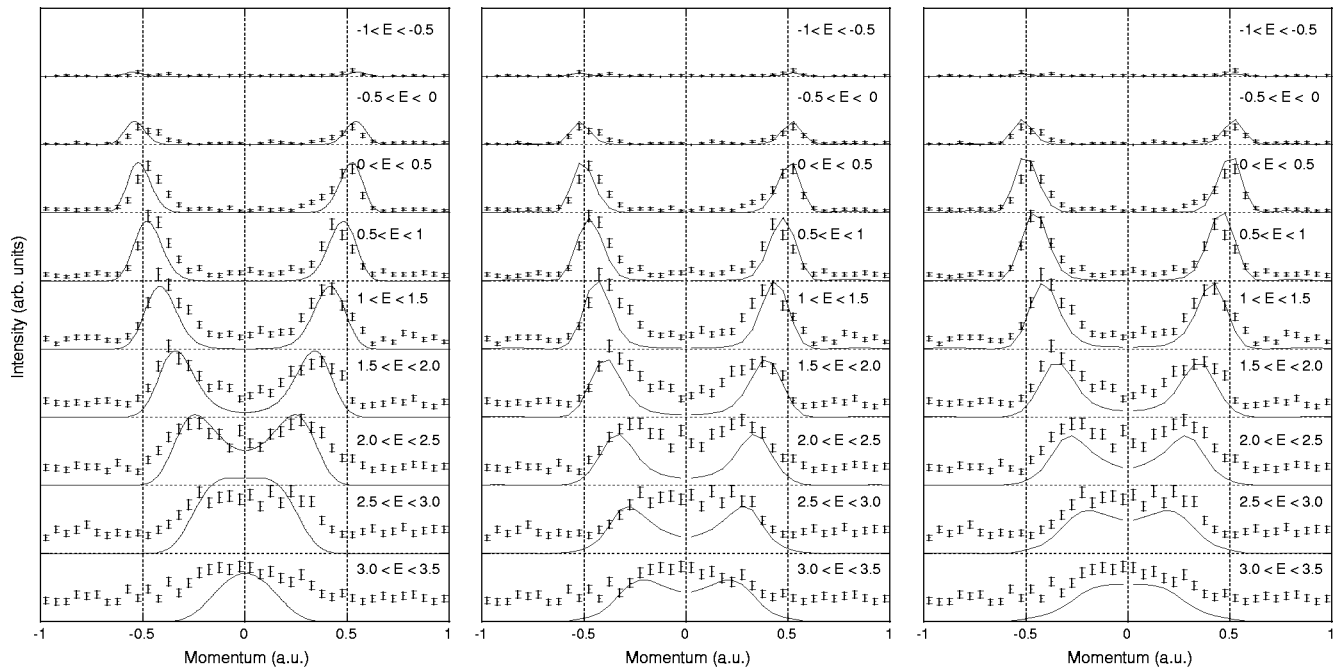
FIG. 10. Measurement of the dispersion of the lithium valence band compared to a free electron band with $m^*=1.6m_e$ and k_F $=0.589$ a.u. (left panel), a cumulant expansion theory not corrected for self-energy effects (central panel) and the same calculation with an energy scale contracted by 20% (right panel).

In the pseudopotential calculations by Northrup *et al.*,[8] who used the *GW* scheme and a modified dielectric function, a good agreement was found between the calculated band width, and that derived from photoemission experiments. In this work the effect of the self-energy correction was a contraction by 15% of the Li binding energy scale. Our experimental bandwidth of 3 eV is in agreement with the photoemission results. As is clear from the central panel of Fig. 10 our self-energy corrections, based on the standard random phase approximation (RPA) of the dielectric function, are too small, in agreement with the findings of others.[8,13] The much larger asymmetry obtained using the cumulant expansion approach causes an apparent shift of the calculated peak to
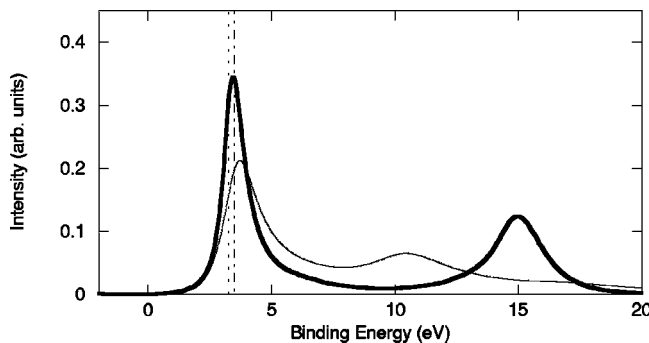

FIG. 11. Calculated spectra for Li at zero momentum using the *GW* approximation (thick line) and the cumulant expansion approach (thin line). The cumulant expansion spectral function peaks at slightly higher binding energy than the density calculated within the *GW* scheme. This is due to the larger asymmetry of the peak. The LDA energy (dash-dotted line) and the LDA energy shifted by the self-energy (short dashed) are shown for comparison.
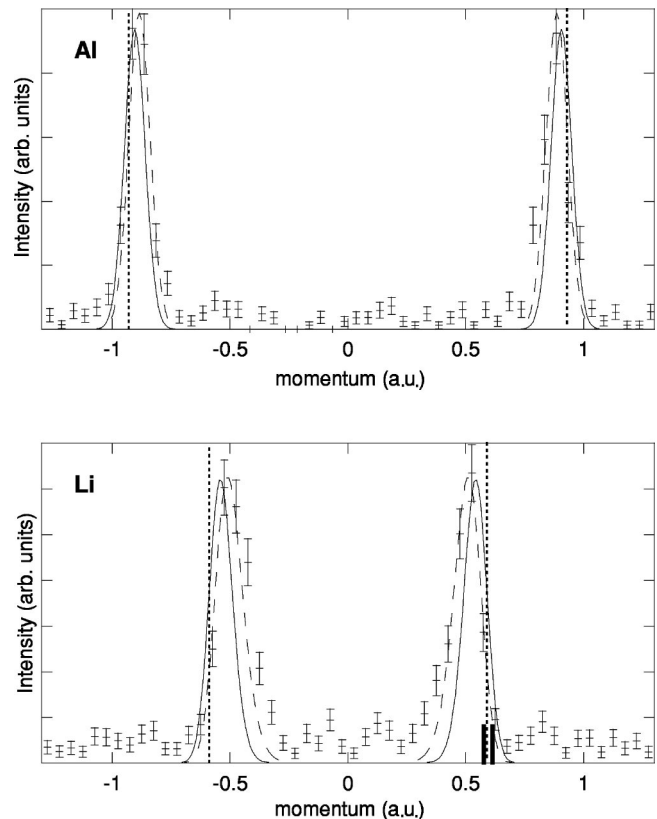
FIG. 12. The measured momentum densities for Al (top) and Li (bottom) at the Fermi level (error bars). The solid line assumes a perfect alignment. The dashed line is obtained by assuming a deviation from the ideal alignment of 0.2 a.u. Two solid bars in the right half of the lithium spectrum indicate the range of the Fermi vectors in the actual solid.

higher binding energies, and hence the required correction due to the real part of the self-energy is even higher (see Fig. 11). The measured quasiparticle line shape and satellite structure is better described by the cumulant expansion approach. In the cumulant expansion approach, using the RPA dielectric function, the calculated band width is too large, even slightly larger than that obtained in the equivalent *GW* scheme.

In the above calculation we assumed a perfect alignment of the spectrometer analyzers and the sample [i.e., $\Theta_1 = \Theta_2 = 44.23°$ (see Fig. 1) the small deviation from 45° is due to relativistic corrections[14]]. In that case we measure along a line in momentum space that intersects the origin. However, due to machining errors and possible stray magnetic fields (in spite of the fact that the whole spectrometer is enclosed in a magnetic shield) the effective scattering geometry could be slightly different. In that case we would measure along a line that does not intersect the origin but has an offset along the p_x, p_z direction. In order to investigate how this could affect the data we assumed an offset of 0.2 a.u. in the p_x, p_z plane. This is about twice the maximum deviation we can expect based on known machining and alignment accuracies. The effect of this misalignment for the aluminum and lithium samples is shown in Fig. 12. Clearly such an misalignment would not affect the aluminum momentum density at k_F, but could explain the somewhat poorer agreement between the measured and calculated spectra of the case of lithium. In that case the bottom of the band would correspond to $|q| = 0.2$ a.u., rather than $|q| = 0$ a.u. In turn this would cause a underestimation of the band width by $(0.2)^2/(2m^*)$, i.e., 0.5 eV for aluminum and 0.3 eV for Li (assuming $m^* = 1.6 m_e$).

Unfortunately in the case of Li we cannot say anything meaningful about the satellite intensity, as the oxygen-derived intensity dominates in this energy-momentum re-gion. The quasiparticle part of the spectral function seems to display the same picture as for aluminum: near the bottom of the band a reduction in the peak height is observed caused by lifetime broadening. The measured dispersion is parabolic to a good approximation. In photoemission data[38] there is remarkably small dispersion of the peaks just below k_F. It is explained as an artifact, due to interference of surface and bulk states. The present measurements does not see any indication of reduced dispersion near k_F and are thus in agreement with the interpretation of the photoemission data by Claesson *et al.*[38]

V. CONCLUSION

We have shown for aluminum that EMS can measure quantitatively the spectral function. For aluminum we start approaching the goal of a quantitative spectroscopy, able to measure the spectral function of core levels and valence band in a uniform way. The one measurement contains the information about dispersion (including self-energy corrections), lifetime broadening, and the density of the quasi-particle and satellite structures for both core and valence band.

For lithium preliminary measurements have shown that the dispersion is close to 3 eV. The intensity distribution over the parabola appears similar to that of aluminum, and hence no obvious direct link to the anomalous Compton results for lithium[6] was found. Momentum profiles at the Fermi level were in agreement with theory within 0.03–0.05 a.u., although for Li the low momentum side of the peaks was somewhat less sharp that expected for a free-electron model, a fact that is, at least in part, due to the asphericity of the Fermi surface of lithium.

The cumulant expansion calculation gives a superior description of the satellite structures and asymmetric line shapes. Some problems remain in describing the band width of these materials correctly.

[1] L. Hedin and S. Lundqvist, Solid State Phys. **23**, 1 (1969).

[2] P. Steiner, H. Höchst, and S. Hüfner, *Photoemission in Solids* (Springer Verlag, Berlin, 1978), Vol. 2, Chap. Simple Metals, p. 349.

[3] L. Hedin, J. Michiels, and J. Inglesfield, Phys. Rev. B **58**, 15 565 (1998).

[4] C. Metz, T. Tschentscher, P. Suortti, A.S. Kheifets, R.D. Lun, T. Sattler, J.R. Schneider, and F. Bell, Phys. Rev. B **59**, 10 512 (1999).

[5] Y. Sakurai, Y. Tanaka, A. Bansil, S. Kaprzyk, A.T. Stewart, Y. Nagashima, T. Hyodo, S. Nanao, H. Kawata, and N. Shiotani, Phys. Rev. Lett. **74**, 2252 (1995).

[6] W. Schülke, G. Stutz, F. Wohlert, and A. Kaprolat, Phys. Rev. B **54**, 14 381 (1996).

[7] C. Sternemann, T. Buslaps, A. Shukla, P. Suortti, G. Döring, and W. Schülke, Phys. Rev. B **63**, 094301 (2001).

[8] J.E. Northrup, M.S. Hybertsen, and S.G. Louie, Phys. Rev. B **39**, 8198 (1989).

[9] I.-W. Lyo and E.W. Plummer, Phys. Rev. Lett. **60**, 1558 (1988).

[10] K.W.-K. Shung, Phys. Rev. B **44**, 13 112 (1991).

[11] D. Claesson, S.-A. Lindgren, and L. Wallden, Phys. Rev. B **60**, 5217 (1999).

[12] N.V. Smith, P. Thiry, and Y. Petroff, Phys. Rev. B **47**, 15 476 (1993).

[13] E.W. Plummer, Phys. Scr. **T17**, 186 (1987).

[14] M. Vos, G.P. Cornish, and E. Weigold, Rev. Sci. Instrum. **71**, 3831 (2000).

[15] M. Vos and E. Weigold, J. Electron Spectrosc. Relat. Phenom. **112**, 93 (2000).

[16] S. Hüfner, *Photoelectron Spectroscopy* (Springer, Berlin, 1995).

[17] M. Cooper, Rep. Prog. Phys. **48**, 415 (1985).

[18] F. Bell and J.R. Schneider, J. Phys.: Condens. Matter **13**, 7905 (2001).

[19] I.E. McCarthy and E. Weigold, Phys. Rep., Phys. Lett. **27C**, 275 (1976).

[20] E. Weigold and I. E. McCarthy, *Electron Momentum Spectroscopy* (Kluwer Academic/Plenum, New York, 1999).

[21] L. Hedin, Phys. Rev. A **139**, A796 (1965).

[22] F. Aryasetiawan and O. Gunnarsson, Rep. Prog. Phys. **61**, 237 (1998).

[23] B. Bergersen, F.W. Klus, and C. Blomberg, Can. J. Phys. **51**, 102 (1973).

[24] L. Hedin, Phys. Scr. **21**, 477 (1980).

[25] C.-O. Almbladh and L. Hedin, *Handbook on Synchrotron Radiation* (North-Holland, Amsterdam, 1983), p. 686.

[26] F. Aryasetiawan, L. Hedin, and K. Karlsson, Phys. Rev. Lett. **77**, 2268 (1996).

[27] M. Vos, A.S. Kheifets, E. Weigold, S.A. Canney, B. Holm, F. Aryasetiawan, and K. Karlsson, J. Phys.: Condens. Matter **11**, 3645 (1999).

[28] M. Vos, A.S. Kheifets, and E. Weigold, J. Phys. Chem. Solids **62**, 2215 (2001).

[29] S.A. Flodstrom, R.Z. Bachrach, R.S. Bauer, and S.B.M. Hagström, Phys. Rev. Lett. **37**, 1282 (1976).

[30] S.A. Canney, M. Vos, A.S. Kheifets, X. Guo, I.E. McCarthy, and E. Weigold, Surf. Sci. **382**, 241 (1997).

[31] M. Vos, A.S. Kheifets, and E. Weigold, J. Electron Spectrosc. Relat. Phenom. **114-116**, 1031 (2001).

[32] M. Vos, A. S. Kheifets, and E. Weigold, in *Correlations, Polarization and Ionization in Atomic Systems*, *IAP Conference Proceedings 604*, edited by D. Madison and M. Schulz (American Institute of Physics, Melville, 2002), pp. 70–75.

[33] B. Lundqvist, Phys. Kondens. Mater. **6**, 193 (1968).

[34] B.S. Itchkawitz, I.-W. Lyo, and E.W. Plummer, Phys. Rev. B **41**, 8075 (1990).

[35] M. Vos, A.S. Kheifets, E. Weigold, and F. Aryasetiawan, Phys. Rev. B **63**, 033108 (2001).

[36] M. Vos and M. Bottema, Phys. Rev. B **54**, 5946 (1996).

[37] R.S. Crisp and S.E. Williams, Philos. Mag. Ser. **8**, 1205 (1960).

[38] D. Claesson, S.-A. Lindgren, L. Wallden, and T.-C. Chiang, Phys. Rev. Lett. **82**, 1740 (1999).